minerals

MDPI

Article

Deformation Features of Super-Deep Diamonds

Alexey Ragozin [1,2,*], Dmitry Zedgenizov [1,2,*], Vladislav Shatsky [1,2], Konstantin Kuper [3] and Hiroyuki Kagi [4]

[1] V.S. Sobolev Institute of Geology and Mineralogy, Siberian Branch Russian Academy of Sciences, Novosibirsk 630090, Russia; shatsky@igm.nsc.ru

[2] Department of Geology and Geophysics, Novosibirsk State University, Novosibirsk 630090, Russia

[3] Budker Institute of Nuclear Physics, Siberian Branch Russian Academy of Sciences, Novosibirsk 630090, Russia; k.e.kuper@inp.nsk.su

[4] Geochemical Research Center, Graduate School of Science, University of Tokyo, Tokyo 113-0033, Japan; kagi@eqchem.s.u-tokyo.ac.jp

* Correspondence: ragoz@igm.nsc.ru (A.R.); zed@igm.nsc.ru (D.Z.)

Received: 22 November 2019; Accepted: 21 December 2019; Published: 24 December 2019

Abstract: The paper presents new data on the internal structure of super-deep (sublithospheric) diamonds from Saõ-Luiz river placers (Brazil) and from alluvial placers of the northeastern Siberian platform (Yakutia). The sublithospheric origin of these diamonds is supported by the presence of mineral inclusions corresponding to associations of the transition zone and lower mantle. The features of morphology and internal structure have been studied by optical and scanning electron microscopy (SEM), cathodoluminescence topography (CL), and electron backscatter diffraction (EBSD) techniques. Diamonds typically have complicated growth histories displaying alternating episodes of growth, dissolution, and post-growth deformation and crushing processes. Most crystals have endured both plastic and brittle deformation during the growth history. Abundant deformation and resorption/growth features suggest a highly dynamic growth environment for super-deep diamonds. High temperatures expected in the transition zone and lower mantle could explain the plastic deformations of super-deep diamonds with low nitrogen content.

Keywords: diamond; internal structure; electron backscatter diffraction; deformation

1. Introduction

Previous studies indicate that most diamonds have been formed at depths of 120–200 km at pressures of 4–6.5 GPa and temperatures of 950–1300 °C [1–6]. However, a small number of diamonds (less than 1% of diamonds worldwide [7]) apparently crystallized at higher depths in the transition zone of the upper mantle (>410 km) or even in the lower mantle (>660 km). These so-called super-deep diamonds seem to form in the sublithospheric mantle either in primary mantle rocks or in subducted mafic rocks of the oceanic lithosphere [8,9]. Mineral inclusions in super-deep diamonds could be divided into three paragenetic groups: (1) metaperidotitic (comparable with the peridotitic upper mantle paragenesis), according to experimental data and study of inclusions in natural super-deep diamonds [10–12] containing ferropericlase (Mg,Fe)O + bridgmanite (Mg,Fe)SiO_3 + jeffbenite (former tetragonal almandine–pyrope phase, TAPP) (Mg,Fe)$_3Al_2Si_3O_{12}$ + Ca-perovskite $CaSiO_3$ + olivine (Mg,Fe)$_2SiO_4$; (2) metabasic (equivalent to the eclogitic upper mantle paragenesis) with majoritic garnet, Ca-perovskite Ca(Si,Ti)O_3, stishovite SiO_2 + Al_2SiO_5, Ca–Al-silicate (CAS), NAL (new aluminum phase) and CF (calcium–ferrite structured phase); and (3) carbonatitic (equivalent to Ca-rich mantle material) comprising Ca-silicates (e.g., merwinite), Ca–Mg–Fe carbonates, and Na–K–Ca carbonates. Hutchison et al. [13] suggested that metabasic diamonds dominate in the transition zone, but the lower mantle mostly carries diamonds with metaperidotitic inclusions. Super-deep diamonds

were reported in various worldwide localities [13–15], i.e., alluvial placers of the Saõ-Luiz river in Brazil [16,17] and northeastern Siberian Platform [18,19].

The study of the internal structure of diamonds for the reconstruction of growth processes remains relevant because of the wide diversity of morphological and mineralogical characteristics of natural diamond crystals. Most of these data concern lithospheric diamonds because of their greater abundance. There is little data regarding the internal structure of super-deep diamonds. Agrosi et al. [20] studied the internal structures of two super-deep diamond samples non-destructively by X-ray diffraction topography (XRDT) and micro Fourier transform infra-red spectroscopy (μFTIR). Results showed that both samples are affected by complex plastic deformation. Hayman et al. [21] explored the internal structure of super-deep diamonds from Rio-Soriso (Brazil) and revealed that examination of cut diamonds under cathodoluminescence topography (CL) provides information about the diamond's history, such as growth conditions, deformation, and resorption. Moreover, in super-deep diamonds, plastic deformation appears around inclusions due to retrograde phase transformations [22,23]. For sublithospheric diamonds, deformation is assumed to be much stronger than that observed in lithospheric diamonds due to greater pressure and temperature. Hence plastic deformation features of diamonds in the sublithospheric mantle may be much more complex and perhaps only distinguished by applying a combination of techniques [20]. In this work, we have studied the internal structures and deformation features of sublithospheric diamonds using multiple specific methods. The results of this study contribute to the understanding of the growth and post-growth histories of such diamonds at the levels of the transition zone and lower mantle.

2. Samples and Methods

In this work, we studied twelve diamonds (1.2–2.3 mm in size) from alluvial placers of São-Luiz (Juina, Brazil) and one diamond from Kholomolokh alluvial placer (northeastern Siberian platform) (Figures 1 and 2). The Juina province (Brazil) is a well-known location with the highest proportion of super-deep diamonds [14,15,17,24–26]. There are also reports of the presence of super-deep diamonds on the Siberian platform [18,19]. Super-deep diamonds from São-Luiz in the present study contain mineral inclusions of majoritic garnet, coesite (suggested former stishovite), Ca–Si-perovskite, ferropericlase, and magnesite (Table 1) [22,25–27]. Majoritic garnet has been detected in diamonds from Kholomolokh [19]. Majoritic garnet inclusions in studied diamonds indicate their formation at different levels of the transition zone, whereas ferropericlase represents the lower mantle association [8,9].

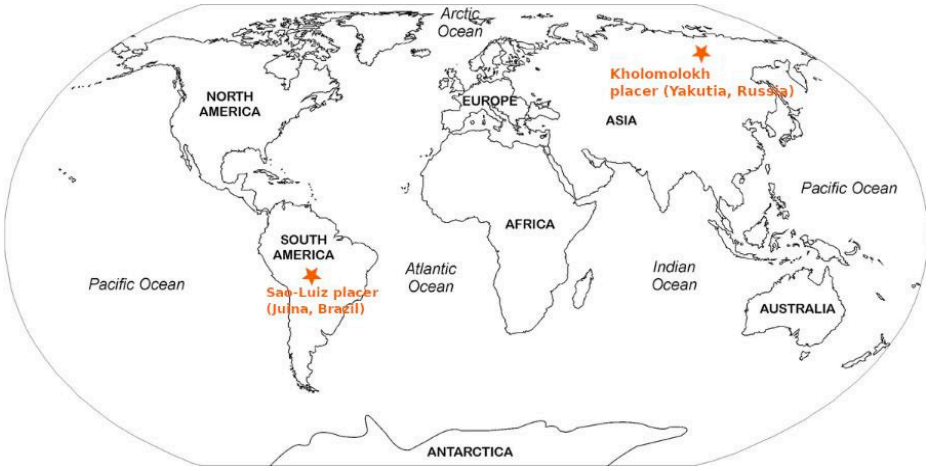

Figure 1. Location map of studied super-deep diamonds.

The morphological features of diamonds were examined by stereomicroscope Zeiss Stemi 506 and scanning electron microscope (SEM) HITACHI TM-1000 (Hitachi High-Technologies Corporation, Tokyo, Japan) installed at Novosibirsk State University with an accelerating voltage of

15 kV and a working distance of 15 mm. Afterward, the crystals were polished into plates 200–400 microns thick to investigate their internal structure.

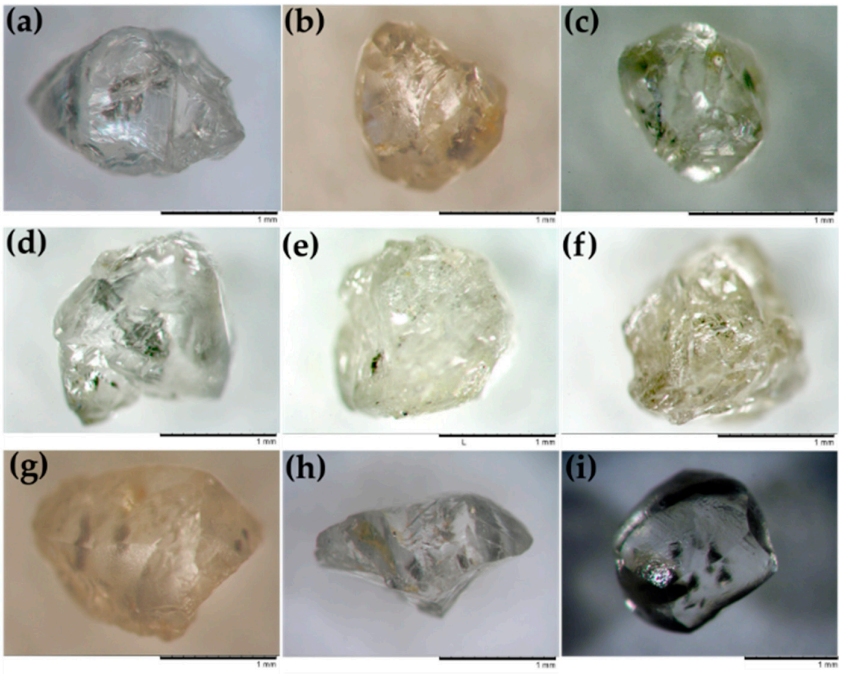

Figure 2. Microphotographs of super-deep diamonds. (**a**) SL-34; (**b**) SL-52; (**c**) SL-55; (**d**) SL-16; (**e**) SL-2; (**f**) SL-24; (**g**) SL-82; (**h**) SL-74; (**i**) HH-11. (a–h) super-deep diamonds from São-Luiz alluvial placers (Juina, Brazil); (i) super-deep diamond crystal from Kholomolokh placer (Yakutia, Russia).

Table 1. Sample description.

Sample	Inclusions	[N_{total}], ppm	%B	Locality
C-2	Maj–Grt	<5 (core)–38 (rim)	100	São-Luiz (Juina, Brazil)
SL-74	Maj–Grt	10 (core)–37 (rim)	100–65	-
SL-52a	Maj–Grt	7 (core)–51 (rim)	100	-
SL-34	Maj–Grt + Ca–Si-Prv	<5 (core)–9 (rim)	100	-
SL-16	Coe + Maj–Grt	25 (core)–38 (rim)	100	-
SL-40	Coe	<5 (core)–8 (rim)	100	-
SL-2	Coe	<5 (core)	-	-
SL-55	Coe + Cpx	<5 (core)–7 (rim)	100	-
SL-82	fPer	<5 (core)	-	-
SL-52	Mgs	<5 (core)	-	-
SL-23	fPer + $CaSiO_3$	<5 (core)–10 (rim)	100	-
SL-24	fPer	14 (core)	100	-
HH-11	Maj–Grt	<5 (core)–115 (rim)	60	Kholomolokh alluvial (Yakutia)

Maj–Grt—majoritic garnet; Ca–Si-Prv—Ca–Si-perovskite; Coe—coesite (former stishovite?); Cpx—clinopyroxene; fPer—ferropericlase; Mgs—magnesite.

Birefringence patterns of polished plates have been observed using a Zeiss Axioscop 40 polarizing microscope. CL patterns of diamond plates were studied using an Oxford Centaurus detector on the SEM Leo-1430VP (accelerating voltages of 12–15 kV and an electron beam current of ~0.5 mA) in the Analytical Center for Multi-Element and Isotope Research SB RAS (Novosibirsk, Russia). The electron backscatter diffraction (EBSD) analysis was performed with the use of the Oxford Instruments HKL detector (Oxford Instruments, Abingdon, Oxfordshire, UK) mounted to a Hitachi S-3400 N scanning electron microscope (SEM) (Hitachi High-Technologies Corporation,

Tokyo, Japan) at an accelerating voltage of 20 kV and a ~1 nA electron beam, with a tilt of 70° and an aperture of 200 μm. Electron backscatter diffraction (EBSD) analysis uses the diffraction patterns generated by the interaction of the SEM electron beam and a crystalline sample to determine the crystallographic orientation of the material. Kikuchi patterns from each individual point were automatically indexed by the Oxford data collection software (Oxford Instruments, Abingdon, Oxfordshire, UK), and the deviation from the basic orientation in the diamond grain was mapped by EBSD. The accuracy of the determination of misorientations by this technique is estimated to be in the range 0.5–1.0°. EBSD was done using the infrastructure of the Shared-Use Center "Siberian Synchrotron and Terahertz Radiation Center (SSTRC)" based on VEPP-3/VEPP-4M/NovoFEL of BINP SB RAS.

Infrared spectra of the studied diamonds were recorded on polished plates using a Bruker Vertex 70 FTIR spectrometer equipped with a HYPERION 2000 microscope in V.S. Sobolev Institute of Geology and Mineralogy (Novosibirsk, Russia). Local spectra were measured using an aperture of 60 × 60 μm in the spectral range of 370–4000 cm^{-1} with 30 scans at a resolution of 2 cm^{-1}, and the content of N-centers was calculated by a standard procedure. The intrinsic absorption of the diamond (12.3 cm^{-1} at 2030 cm^{-1}) was taken to be the internal standard [28]. The content of N-defects was determined by the ratios proposed in [29–31].

3. Results and Discussion

3.1. Morphology

The diamonds were presented by single crystals and intergrowths (Figure 3). Some samples were flattened and elongated (e.g., SL-16) or distorted in other ways (e.g., SL-24). Several diamonds were intergrowths of crystals with the same morphological features (e.g., SL-2). Diamond SL-16 (Figure 3d) had a Star of David shape, which represents the peritropic twin of two crystals orientated by spinel law at 180° to each other [32]. Some diamonds (e.g., SL-55, SL-16, SL-82; Figure 3c,d,h) were mechanically broken or damaged.

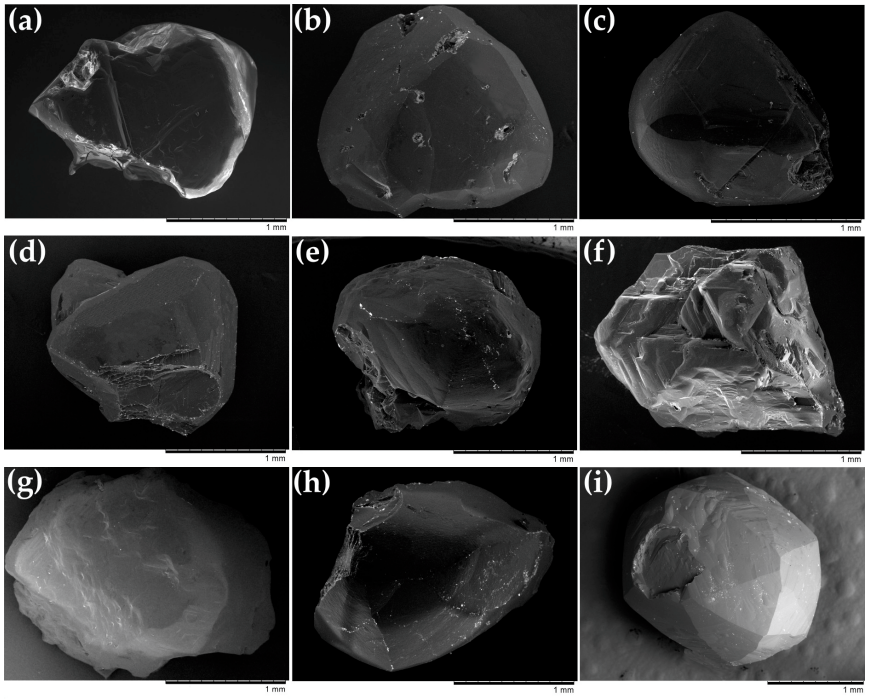

Figure 3. Morphology of studied super-deep diamonds (backscattered electron image). (**a**) SL-34; (**b**) SL-52; (**c**) SL-55; (**d**) SL-16; (**e**) SL-2; (**f**) SL-24; (**g**) C-2; (**h**) SL-82; (**i**) HH-11. (a–h) super-deep diamonds from São-Luiz alluvial placers (Juina, Brazil); (i) super-deep diamond crystal from Kholomolokh placer (Yakutia, Russia).

The crystals showed typical resorption features and retained only relics of primary growth morphologies [33–37]. The primary octahedral morphology manifested in many studied samples (e.g., SL-34, SL-55, SL-16; Figure 3a,c,d). These crystals have convex rounded surfaces observed near the crystal edges, which suggest their partial resorption. The shape of these crystals represents the transition from octahedron and rounded rhombic dodecahedron (so-called dodecahedroid). The relics of octahedral faces often show deep trigonal etch-pits (Figure 4a,b). The trigonal etch-pits are oriented in the opposite direction from the underlying face (negative trigons [38]). The number and size of the negative trigons, which differ even in individual crystals, may be caused by dislocations of different types and with impurity agglomerations, microcracks, and other surface defects [39,40].

Resorbed rounded surfaces generally developing on the edges of octahedral crystals correspond to the dodecahedroid or tetrahexahedroid shape. These shapes are extreme resorption forms observed in experiments [34,35], and they are common for many natural diamonds [41–43]. Diamond HH-11 (Figure 3i) from Kholomolokh alluvial deposit (Yakutia, Russia) is a typical rounded crystal of predominantly tetrahexahedroid shape (Figure 3f). The characteristic microrelief features of resorbed rounded surfaces are striations and drop-shaped hillocks (Figure 4c,d).

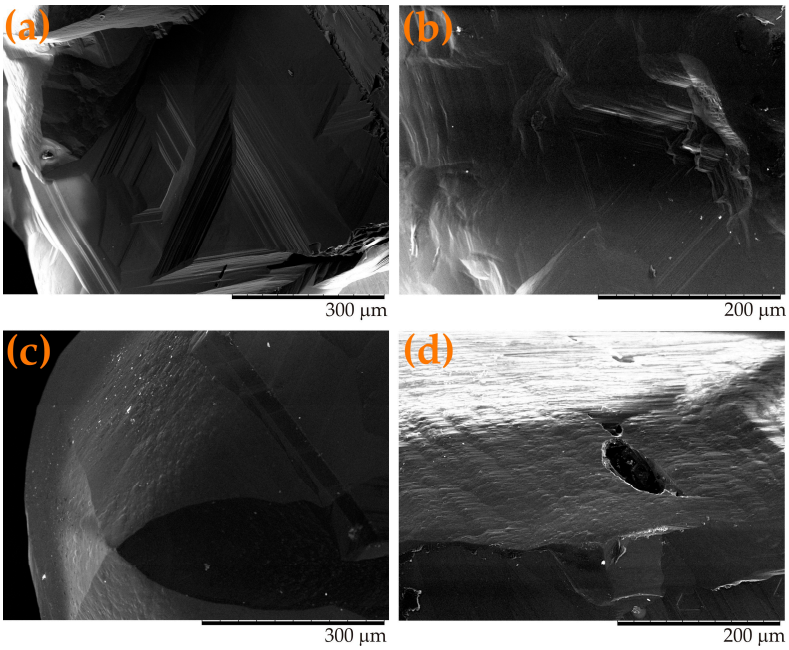

Figure 4. Surface microrelief features of super-deep diamonds (backscattered electron image). (**a**) Triangular etch pits on the relics of (111) plane, Sample HH-11; (**b**) Sample SL-34; (**c**) drop-shaped hillocks on the rounded surface of SL-2 diamond; (**d**) striation on the rounded surface of SL-55 diamond.

3.2. IR Characteristics

Nitrogen is the most common structural impurity in natural diamonds [44]. Based on the nitrogen content detected by IR spectroscopy, diamonds are classified into nitrogen-containing type I and nitrogen-free type II [45–47]. Generally, type I diamonds can contain C-, A-, and B-centers [45]. Type Ib diamonds contain single substitutional nitrogen atoms in the diamond lattice (C-center), representing the initial stage of nitrogen incorporation into the lattice of the diamond according to the theory of transformation of nitrogen defects in diamonds as a function of temperature and annealing time [48–51]. Type IIa diamonds are almost or entirely devoid of impurities whereas type IIb diamonds contain significant boron impurities. Type IaA diamonds are characterized by a pair of nitrogen atoms (A-center) substituting for two carbon atoms in adjacent positions of the crystal lattice [52], representing the second stage of nitrogen aggregation. Finally, four nitrogen atoms tetrahedrally arranged around a vacancy (B-center) [53] and B'-center or platelets, with a planar defect consisting

of interstitial carbon atoms, probably decorated with nitrogen atoms [54]. Diamonds of type IaB are the final stage of nitrogen aggregation. The nitrogen concentration and aggregation state may reflect the conditions of diamond formation and their subsequent thermal evolution [44].

Nitrogen characteristics of super-deep diamonds from the São-Luiz alluvial deposit were previously described in [55–57]. FTIR spectroscopy has revealed local variations in nitrogen defects in diamonds from São-Luiz and Kholomolokh alluvial placers (Table 1). Diamonds from São-Luiz contain less than 51 ppm of nitrogen; in fact, many of them have zones with no detectable (<5 ppm) nitrogen and thus can be classified as type IIa. Previous studies have revealed the high proportion of nitrogen-free type II diamonds among super-deep diamonds [8,10–13]. The studied diamonds with detectable nitrogen were characterized by an extremely high nitrogen aggregation state (100% of B centers in most cases, type IaB diamonds) due to high temperatures of the transition zone and lower mantle. The presence of a band centered at 3107 cm^{-1} and attributed to hydrogen-containing defects [58] was detected only in diamonds containing nitrogen. Figure 5 depicts the representative FTIR spectra of super-deep diamonds (SL-52). The core of this diamond contains less than 7 ppm of nitrogen, whereas the rim has 50 ppm of totally aggregated nitrogen (pure IaB-type) accompanied with a higher-intensity 3107 cm^{-1} band. Diamond HH-11 from Kholomolokh alluvial placers had an internal zone containing no nitrogen (type II), whereas the nitrogen concentration in the outer zone reaches 115 ppm with an aggregation state of ~60%B [19].

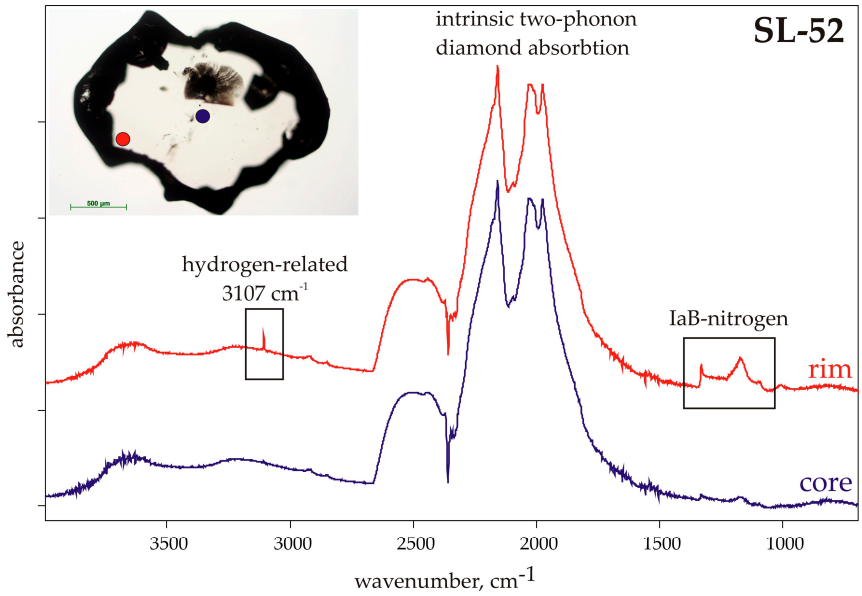

Figure 5. Representative Fourier transform infra-red (FTIR) spectra of core (dark-blue) and rim (red) of diamond SL-52. The locations of each spectra are highlighted on the transmitted light image of the polished plate (left corner).

3.3. Birefringence

Birefringence in diamonds is an anomalous optical property. The interference pattern of anomalous birefringence is not expected in minerals of cubic syngony and may indicate a high degree of deformation of their crystal structure. Its appearance in diamonds is the result of lattice strains, modifying its natural isotropic properties [59,60]. Polarized microscopy observation of polished plates of super-deep diamonds shows anomalous birefringence patterns that may be related to deformation features of studied diamonds (Figure 6). The birefringence patterns of some studied diamonds have a specific "tatami" configuration, which is attributed to plastic deformation [60–62]. The birefringent lamellae are crystallographically defined and commonly occur parallel to an octahedral plane. In some samples, there can be more than one set of intersecting lamellae (e.g., samples SL-34, SL-82; Figure 6a,h), running parallel to different sets of octahedral planes.

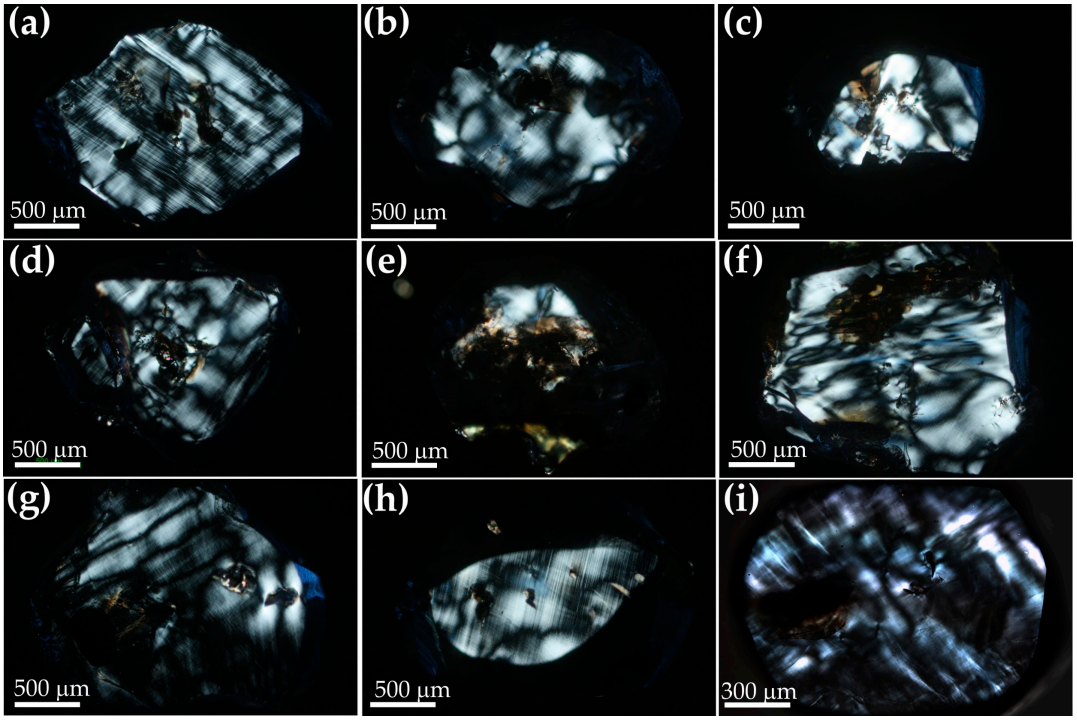

Figure 6. Birefringence patterns of double-polished plates from super-deep diamonds. (**a**) SL-34; (**b**) SL-52; (**c**) SL-55; (**d**) SL-16; (**e**) SL-2; (**f**) SL-24; (**g**) C-2; (**h**) SL-82; (**i**) HH-11. (a–h) super-deep diamonds from São-Luiz alluvial placers (Juina, Brazil); (i) super-deep diamond crystal from Kholomolokh placer (northeastern Siberian Platform).

3.4. Cathodoluminescence

Cathodoluminescence (CL) images of diamonds help to visualize zonation and growth sectors, apparently due to different distributions of impurities of nitrogen and other structural defects [62,63]. CL images of the polished plates of the diamonds studied here visualize their complex growth histories (Figure 7). The crystals typically show several contrasting growth zones that may have thin-layered concentric zoning. The profiles of growth zones often have an irregular shape indicating that the morphology was distorted from the initiation of crystal growth. Many samples exhibit elements of octahedral zonation. Various zones of the crystals have traces of plastic deformations as a series of thin lines (deformation lamellae) intersecting different growth zones of the crystals. These features of the internal structure have also been detected in many previously described super-deep diamonds derived from different depth regimes [10,12,15,20,56,64–66].

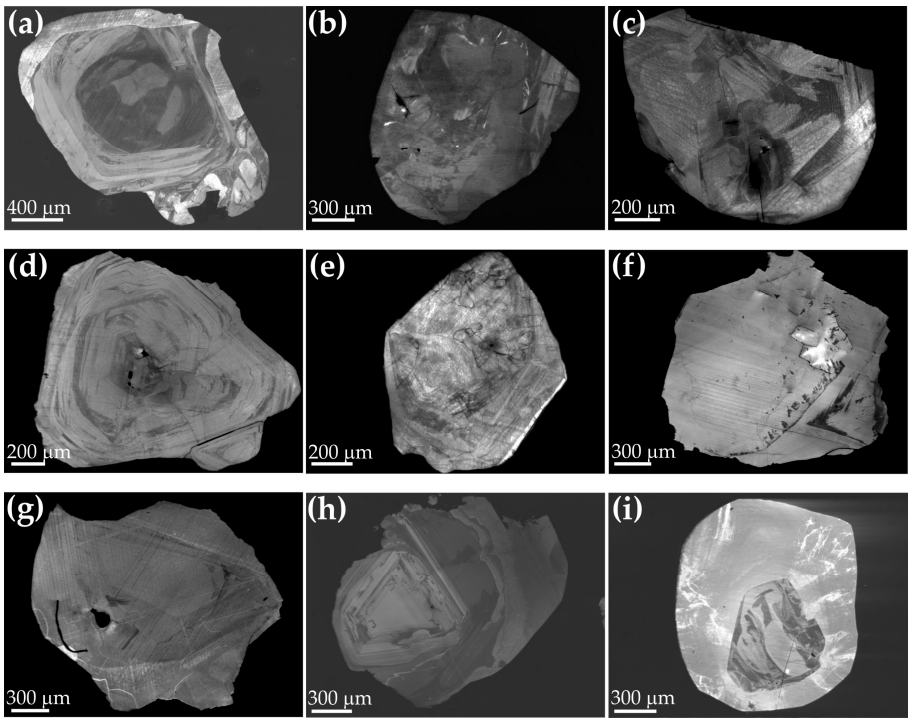

Figure 7. Cathodoluminescence images of polished plates of super-deep diamonds from São-Luiz deposit, Brazil: (a-h) and Kholomolokh alluvial placer (Yakutia): (i). (**a**) SL-34; (**b**) SL-52; (**c**) SL-55; (**d**) SL-16; (**e**) SL-2; (**f**) SL-24; (**g**) C-2; (**h**) SL-82; (**i**) HH-11. (a–h) super-deep diamonds from São-Luiz alluvial placers (Juina, Brazil); (i) super-deep diamond crystal from Kholomolokh placer (Yakutia, Russia).

CL images of many diamonds from São-Luiz suggest fluctuations in their growth and post-growth histories. For example, samples SL-34, SL-16, and SL-82 (Figure 7a,d,h) show oscillating zonation with alternating flat octahedral growth zones and curved resorbed surfaces. In some studied crystals, CL has revealed evidence of brittle deformation (Figure 7c,d,e). Such evidence of brittle deformation includes displaced growth zones and dissolution surfaces along internal healed cracks; however, these do not extend to the surface of the crystals. These healed cracks are terminated by younger growth zones, indicating that they appeared before diamond growth was complete or between distinct growth events. Diamond HH-11 from Kholomolokh is distinguished by two distinct zones (Figure 7d) and a majoritic garnet at its core.

This study has revealed episodes of growth and dissolution in most studied super-deep diamonds. Other common features are plastic and brittle deformations. Brittle deformation took place at the different stages of the formation of the studied diamonds. A shift of growth zones along fractures in some diamonds indicates brittle strains between different growth episodes. Such brittle deformations could occur at different stages of crystal formation, but, in many cases, the crystals have undisturbed outer growth zones. The episodes of growth, dissolution, and deformation may proceed at different levels in the transition zone and lower mantle, as suggested by the mineral inclusions.

3.5. EBSD

The EBSD technique is generally employed for precise determination of textural features of crystals expressed as the lattice orientation relationships between the crystal blocks. Misorientation of the diamond structure immediately around the inclusions ranges from 2° to 5°, as previously described in [22,23]. It has been used as the evidence for phase transitions in mineral inclusions of bridgmanite, CaSi- and CaTiSi-perovskites, SiO_2 (stishovite?), and Mg_2SiO_4 (ringwoodite?) [22]. The absence of deformation near ferropericlase and majoritic garnet inclusions suggests the lack of phase transitions with dramatic volume changes.

In this study, we used the EBSD technique to analyze the misorientations of crystal structure in super-deep diamonds (Figures 8–10). The studied diamonds have a mosaic internal structure and, in some cases, consist of several units (blocks or subindividuals). Deformation lines are observed in many studied diamonds (Figures 8b,c,d and 9). Some samples demonstrate several subindividuals significantly misorientated to each other up to 60° (Figure 10a,b). The misorientations at such significant angles certainly testify to the polycrystalline texture of these samples. Most likely, they were initially formed as intergrowths or aggregates. Nevertheless, evidence of plastic deformation, which is expressed in the form of small misorientations of the crystal structure of diamonds, is recorded inside the single subindividuals of the intergrowths (Figure 10c,d).

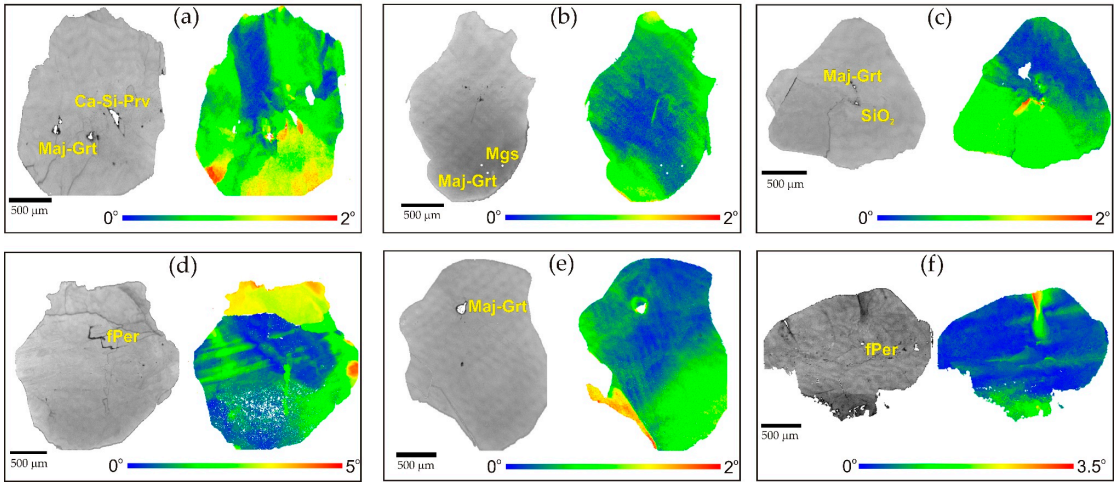

Figure 8. Misorientation patterns of super-deep diamonds from São-Luiz alluvial placers (Juina, Brazil). Electron backscatter diffraction (EBSD) maps over large parts of the polished plates showing a change in orientation. (**a**) SL-34; (**b**) SL-55; (**c**) SL-16; (**d**) SL-24; (**e**) C-2; (**f**) SL-82 (left—reflected light, right—EBSD image, bottom—misorientation degrees).

Within individual crystals (or subindividuals), the lattice misorientation can reach up to 5° but is usually less than 2°. These misorientations within the diamond crystals result from the plastic deformation that can occur during growth and post-growth stages. It has been shown that nitrogen-containing diamond deforms plastically and fractures more easily for a given set of experimental conditions than diamonds with very low levels of nitrogen but high dislocation densities [67]. The expected temperatures for the formation of super-deep diamonds in the transition zone and lower mantle (1400–1600 °C and more) are significantly higher than those defined for "ordinary" lithospheric diamonds (950–1300 °C). These higher temperatures could explain why even nitrogen-free super-deep diamonds can easily be plastically deformed.

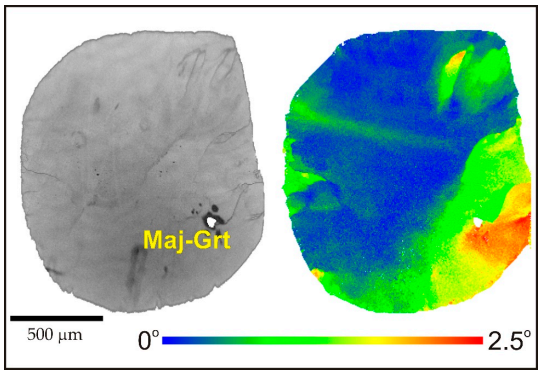

Figure 9. Misorientation pattern of super-deep diamond HH-11 from Kholomolokh alluvial placers (Yakutia, Russia) (left—reflected light, right—EBSD image, bottom—misorientation degrees).

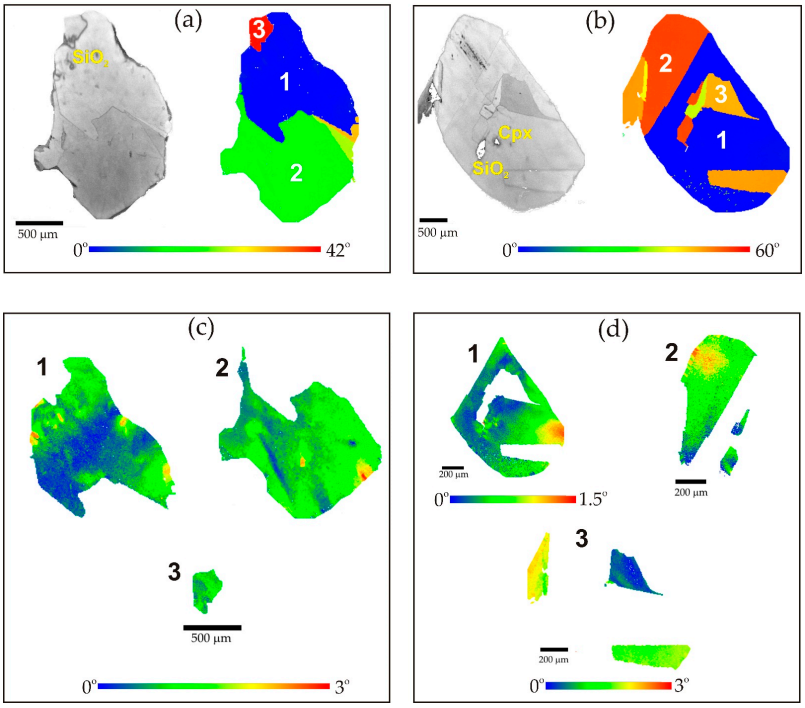

Figure 10. Misorientation patterns of super-deep diamonds with large misorientations of subindividuals from São-Luiz alluvial placers (Juina, Brazil). EBSD maps over large parts of the polished plates showing a change in orientation. (left—reflected light, right—EBSD image, bottom—misorientation degrees). (**a,c**) SL-2; (**b,d**) SL-55. (a,b) EBSD maps over large parts of the polished plates showing a change in orientation. (c,d) EBSD maps of single subindividuals of samples.

A combination of different analytical techniques (CL, birefringence imaging, IR spectroscopy as well as EBSD) was used to improve understanding of the effects of plastic deformation on nitrogen aggregation, impurity and defect migration in diamonds [67]. Evans and Wild [68] suggested that in a bend experiment, the transition between brittle and ductile behavior for type II diamonds occurs within the temperature range of 1400 to 1600 °C. According to these data, we suggest that brittle deformation of super-deep diamonds could occur in subduction zones because of the relatively low temperatures in the slab. New results on deformations in super-deep diamonds could potentially be applied to establish specific geological processes in the transition zone and lower mantle. Some of the observed deformation features, however, could be attributed to the ascent of the diamond through shallower parts of the mantle (within a kimberlite or precursor melt) rather than processes occurring in the lower mantle/transition zone.

4. Conclusions

The internal structures and deformation features of super-deep diamonds have been studied by several methods. These diamonds contain mineral inclusions that indicate their formation at different levels of the transition zone and lower mantle association. The super-deep diamonds were of an irregular shape with signs of partial dissolution. These diamonds contained either no nitrogen (type IIa) or a low amount of nitrogen in an extremely aggregated form (Type IaB). All studied diamonds contained defects, such as inclusions or microcracks, and had strained internal structures, which can be attributed to plastic deformation. CL has revealed episodes of growth, dissolution, and deformation (both plastic and brittle) in many super-deep diamonds. These episodes may occur at different levels in the transition zone and lower mantle. EBSD demonstrates a mosaic internal structure of diamonds with misorientation up to 5° (usually less than 2°) within an individual crystal (or blocks). These misorientations result from the plastic deformation that appears in diamonds during growth and post-growth stages at high temperatures. The nitrogen-containing diamond

deforms plastically and fractures more easily, for a given set of experimental conditions, than diamonds with very low levels of nitrogen but high dislocation densities. Abundant deformation and resorption/growth features suggest a highly dynamic growth environment for super-deep diamonds. Higher temperatures expected in the transition zone and lower mantle could explain the plastic deformations of super-deep diamonds with low nitrogen content.

Author Contributions: Conceptualization, A.R. and D.Z.; Formal analysis, H.K.; Investigation, A.R., D.Z. and K.K.; Methodology, K.K.; Resources, H.K.; Supervision, V.S.; Validation, V.S. and K.K.; Writing—original draft, A.R. and D.Z.

Funding: Work is done on state assignment of IGM SB RAS. The research was supported in part by RFBR (project No. 18-05-70014).

Conflicts of Interest: The authors declare no conflict of interest.

References

1. Sobolev, N.V. *Deep Seated Inclusions in Kimberlites and the Problem of the Composition of the Upper Mantle*; AGU: Washington, DC, USA, 1977; p. 279.
2. Meyer, H.O.A. Genesis of diamond—A mantle saga. *Am. Miner.* **1985**, *70*, 344–355.
3. Meyer, H.O.A. Inclusions in diamond. In *Mantle Xenoliths*; Nixon, P.H., Ed.; Wiley: Chichester, NJ, USA, 1987; pp. 501–522.
4. Bulanova, G.P. The formation of diamond. *J. Geochem. Explor.* **1995**, *53*, 1–23.
5. Stachel, T.; Harris, J.W. The origin of cratonic diamonds—Constraints from mineral inclusions. *Ore Geol. Rev.* **2008**, *34*, 5–32.
6. Stachel, T.; Luth, R.W. Diamond formation—Where, when and how? *Lithos* **2015**, *220*, 200–220.
7. Stachel, T. Diamonds from the asthenosphere and the transition zone. *Eur. J. Mineral.* **2001**, *13*, 883–892.
8. Harte, B. Diamond formation in the deep mantle: The record of mineral inclusions and their distribution in relation to mantle dehydration zones. *Mineral. Mag.* **2010**, *74*, 189–215, doi:10.1180/minmag.2010.074.2.189.
9. Harte, B. Diamond Window into the Lower Mantle. *Science* **2011**, *333*, 51–52, doi:10.1126/science.1213012.
10. Bulanova, G.P.; Walter, M.J.; Smith, C.B.; Kohn, S.C.; Armstrong, L.S.; Blundy, J.; Gobbo, L. Mineral inclusions in sublithospheric diamonds from Collier 4 kimberlite pipe, Juina, Brazil: Subducted protoliths, carbonated melts and primary kimberlite magmatism. *Contrib. Mineral. Petrol.* **2010**, *160*, 489–510, doi:10.1007/s00410-010-0490-6.
11. Kaminsky, F. Mineralogy of the lower mantle: A review of 'super-deep' mineral inclusions in diamond. *Earth-Sci. Rev.* **2012**, *110*, 127–147, doi:10.1016/j.earscirev.2011.10.005.
12. Kaminsky, F.V.; Zakharchenko, O.D.; Davies, R.; Griffin, W.L.; Khachatryan-Blinova, G.K.; Shiryaev, A.A. Superdeep diamonds from the Juina area, Mato Grosso State, Brazil. *Contrib. Mineral. Petrol.* **2001**, *140*, 734–753.
13. Hutchison, M.T.; Hursthouse, M.B.; Light, M.E. Mineral inclusions in diamonds: Associations and chemical distinctions around the 670-km discontinuity. *Contrib. Mineral. Petrol.* **2001**, *142*, 119–126.
14. Harte, B.; Harris, J.; Hutchison, M.; Watt, G.; Wilding, M. Lower mantle mineral associations in diamonds from Sao Luiz, Brazil. In *Mantle Petrology: Field Observations and High-Pressure Experimentation: A Tribute to Francis R. (Joe) Boyd*; The Geochemical Society: Houston, TX, USA, 1999; Volume 6, pp. 125–153.
15. Hutchison, M.; Cartigny, P.; Harris, J. Carbon and nitrogen compositions and physical characteristics of transition zone and lower mantle diamonds from Sao Luiz, Brazil. In *Proceedings of the VII International Kimberlite Conference, University of Cape Town, South Africa, 11–17 April 1998*; Red Roof Design: Cape Town, South Africa, 1999; Volume 2, pp. 372–382.
16. Joswig, W.; Stachel, T.; Harris, J.W.; Baur, W.H.; Brey, G.P. New Ca-silicate inclusions in diamonds—Tracers from the lower mantle. *Earth Planet. Sci. Lett.* **1999**, *173*, 1–6.
17. McCammon, C.; Hutchison, M.; Harris, J. Ferric iron content of mineral inclusions in diamonds from Sao Luiz: A view into the lower mantle. *Science* **1997**, *278*, 434–436, doi:10.1126/science.278.5337.434.
18. Sobolev, N.V.; Logvinova, A.M.; Zedgenizov, D.A.; Seryotkin, Y.V.; Yefimova, E.; Floss, C.; Taylor, L. Mineral inclusions in microdiamonds and macrodiamonds from kimberlites of Yakutia: A comparative study. *Lithos* **2004**, *77*, 225–242.

19. Shatskii, V.S.; Zedgenizov, D.A.; Ragozin, A.L. Majoritic garnets in diamonds from placers of the Northeastern Siberian Platform. *Dokl. Earth Sci.* **2010**, *432*, 835–838, doi:10.1134/s1028334x10060279.
20. Agrosì, G.; Tempesta, G.; Della Ventura, G.; Cestelli Guidi, M.; Hutchison, M.; Nimis, P.; Nestola, F. Non-Destructive In Situ Study of Plastic Deformations in Diamonds: X-ray Diffraction Topography and μFTIR Mapping of Two Super Deep Diamond Crystals from São Luiz (Juina, Brazil). *Crystals* **2017**, *7*, 233.
21. Hayman, P.C.; Kopylova, M.G.; Kaminsky, F.V. Lower mantle diamonds from Rio Soriso (Juina area, Mato Grosso, Brazil). *Contrib. Mineral. Petrol.* **2005**, *149*, 430–445.
22. Zedgenizov, D.A.; Shatsky, V.S.; Panin, A.V.; Evtushenko, O.V.; Ragozin, A.L.; Kagi, H. Evidence for phase transitions in mineral inclusions in superdeep diamonds of the Sao Luiz deposit (Brazil). *Rus. Geol. Geophys.* **2015**, *56*, 296–305, doi:10.1016/j.rgg.2015.01.021.
23. Cayzer, N.J.; Odake, S.; Harte, B.; Kagi, H. Plastic deformation of lower mantle diamonds by inclusion phase transformations. *Eur. J. Mineral.* **2008**, *20*, 333–339.
24. Wilding, M.C.; Harte, B.; Harris, J.W. Evidence for a deep origin for the Sao Luiz diamonds. In Proceedings of the 5th International Kimberlite Conference, Araxa, Brazil, 18 June–4 July 1991; pp. 456–458.
25. Harris, J.; Hutchison, M.T.; Hursthouse, M.; Light, M.; Harte, B. A new tetragonal silicate mineral occurring as inclusions in lower-mantle diamonds. *Nature* **1997**, *387*, 486–488, doi:10.1038/387486a0.
26. Zedgenizov, D.A.; Ragozin, A.L.; Kalinina, V.V.; Kagi, H. The mineralogy of Ca-rich inclusions in sublithospheric diamonds. *Geochem. Int.* **2016**, *54*, 890–900, doi:10.1134/s0016702916100116.
27. Zedgenizov, D.A.; Ragozin, A.L.; Kagi, H.; Yurimoto, H.; Shatsky, V.S. SiO_2 Inclusions in Sublithospheric Diamonds. *Geochem. Int.* **2019**, *57*, 964–972, doi:10.1134/S0016702919090131.
28. Zaitsev, A.M. *Optical Properties of Diamond. A Data Handbook*; Springer: Berlin/Heidelberg, Germany, 2001; 502p.
29. Boyd, S.R.; Kiflawi, I.; Woods, G.S. The relationship between infrared absorption and the A defect concentration in diamond. *Philos. Mag. B* **1994**, *69*, 1149–1153.
30. Boyd, S.; Kiflawi, I.; Woods, G. Infrared absorption by the B nitrogen aggregate in diamond. *Philos. Mag. B* **1995**, *72*, 351–361.
31. Woods, G.S.; Purser, G.C.; Mtimkulu, A.S.S.; Collins, A.T. The nitrogen-content of type Ia natural diamonds. *J. Phys. Chem. Solids* **1990**, *51*, 1191–1197, doi:10.1016/0022-3697(90)90101-k.
32. Yacoot, A.; Moore, M.; Machado, W.G. Twinning in Natural Diamond. I. Contact Twins. *J. Appl. Crystallogr.* **1998**, *31*, 767–776, doi:10.1107/S0021889898005317.
33. Khokhryakov, A.F.; Palyanov, Y.N. Effect of crystal defects on diamond morphology during dissolution in the mantle. *Am. Miner.* **2015**, *100*, 1528–1532.
34. Khokhryakov, A.F.; Pal'yanov, Y.N. The evolution of diamond morphology in the process of dissolution: Experimental data. *Am. Miner.* **2007**, *92*, 909–917, doi:10.2138/am.2007.2342.
35. Khokhryakov, A.F.; Pal'yanov, Y.N. Influence of the fluid composition on diamond dissolution forms in carbonate melts. *Am. Miner.* **2010**, *95*, 1508–1514, doi:10.2138/am.2010.3451.
36. Yamaoka, S.; Kanda, H.; Setaka, N. Etching of diamond octahedrons at high temperatures and pressure with controlled oxygen partial pressure. *J. Mater. Sci.* **1980**, *15*, 332–336.
37. Harris, J.; Vance, E. Studies of the reaction between diamond and heated kimberlite. *Contrib. Mineral. Petrol.* **1974**, *47*, 237–244.
38. Frank, F.C.; Puttick, K.E.; Wilks, E.M. Etch pits and trigons on diamond: I. *Philos. Mag.* **1958**, *3*, 1262–1272, doi:10.1080/14786435808233308.
39. Khokhryakov, A.F.; Palyanov, Y.N. Revealing of dislocations in diamond crystals by the selective etching method. *J. Cryst. Growth* **2006**, *293*, 469–474, doi:10.1016/j.jcrysgro.2006.05.044.
40. Lang, A.R. Dislocations in diamond and the origin of trigones. *Proc. R. Soc. Lond. Ser. A. Math. Phys. Sci.* **1964**, *278*, 234–242.
41. Moore, M.; Lang, A.R. On the origin of the rounded dodecahedral habit of natural diamond. *J. Cryst. Growth* **1974**, *26*, 133–139, doi:10.1016/0022-0248(74)90213-9.
42. Machado, W.; Moore, M.; Woods, G. On the dodecahedral growth of coated diamonds. *J. Cryst. Growth* **1985**, *71*, 718–727.
43. Ragozin, A.L.; Zedgenizov, D.A.; Kuper, K.E.; Shatsky, V.S. Radial mosaic internal structure of rounded diamond crystals from alluvial placers of Siberian platform. *Mineral. Petrol.* **2016**, *110*, 861–875, doi:10.1007/s00710-016-0456-0.

44. Evans, T. Aggregation of nitrogen in diamond. In *Properties of Natural and Synthetic Diamond*; Field, J.E., Ed.; Elsevier Academic Press: Amsterdam, The Netherlands; 1992; pp. 259–289.
45. Robertson, R.; Fox, J.J.; Martin, A. Two types of diamond. *Philos. Trans. R. Soc. Lond. Ser. A Contain. Pap. Math. Phys. Character* **1933**, *232*, 463–535.
46. Robertson, R.; Fox, J.J.; Martin, A. Further work on two types of diamond. *Proc. R. Soc. Lond. Ser. A-Math. Phys. Sci.* **1936**, *157*, 579–593.
47. Kaiser, W.; Bond, W. Nitrogen, a major impurity in common type I diamond. *Phys. Rev.* **1959**, *115*, 857.
48. Chrenko, R.; Tuft, R.; Strong, H. Transformation of the state of nitrogen in diamond. *Nature* **1977**, *270*, 141–144.
49. Evans, T.; Qi, Z. The kinetics of the aggregation of nitrogen atoms in diamond. *Proc. R. Soc. Lond. Ser. A-Math. Phys. Eng. Sci.* **1982**, *381*, 159–178.
50. Taylor, W.R.; Canil, D.; Milledge, H.J. Kinetics of Ib to IaA nitrogen aggregation in diamond. *Geochim. Cosmochim. Acta* **1996**, *60*, 4725–4733.
51. Fallon, P.J.; Brown, L.M.; Barry, J.C.; Bruley, J. Nitrogen determination and characterization in natural diamond platelets. *Philos. Mag. A* **1995**, *72*, 21–37, doi:10.1080/01418619508239580.
52. Davies, G. The A nitrogen aggregate in diamond-its symmetry and possible structure. *J. Phys. C Solid State Phys.* **1976**, *9*, L537.
53. Bursill, L.A.; Glaisher, R.W. Aggregation and dissolution of small and extended defect structures in type Ia diamond. *Am. Miner.* **1985**, *70*, 608–618.
54. Speich, L.; Kohn, S.C.; Wirth, R.; Bulanova, G.P.; Smith, C.B. The relationship between platelet size and the B′-infrared peak of natural diamonds revisited. *Lithos* **2017**, *278–281*, 419–426, doi:10.1016/j.lithos.2017.02.010.
55. Zedgenizov, D.A.; Shatskiy, A.; Ragozin, A.L.; Kagi, H.; Shatsky, V.S. Merwinite in diamond from Sao Luiz, Brazil: A new mineral of the Ca-rich mantle environment. *Am. Miner.* **2014**, *99*, 547–550.
56. Zedgenizov, D.; Kagi, H.; Shatsky, V.; Ragozin, A. Local variations of carbon isotope composition in diamonds from São-Luis (Brazil): Evidence for heterogenous carbon reservoir in sublithospheric mantle. *Chem. Geol.* **2014**, *363*, 114–124.
57. Yuryeva, O.P.; Rakhmanova, M.I.; Nadolinny, V.A.; Zedgenizov, D.A.; Shatsky, V.S.; Kagi, H.; Komarovskikh, A.Y. The characteristic photoluminescence and EPR features of superdeep diamonds (São-Luis, Brazil). *Phys. Chem. Miner.* **2015**, *42*, 707–722.
58. Woods, G.S.; Collins, A.T. Infrared absorption spectra of hydrogen complexes in type I diamonds. *J. Phys. Chem. Solids* **1983**, *44*, 471–475, doi:10.1016/0022-3697(83)90078-1.
59. Howell, D. Strain-induced birefringence in natural diamond: A review. *Eur. J. Mineral.* **2012**, *24*, 575–585.
60. Lang, A.R. Causes of birefringence in diamond. *Nature* **1967**, *213*, 248–251.
61. Orlov, Y.L. *The Mineralogy of Diamond*; John Wiley: New York, NY, USA, 1977; 233p.
62. Lang, A.R. Topographic methods for studying defects in diamonds. *Diam. Relat. Mat.* **1993**, *2*, 106–114, doi:10.1016/0925-9635(93)90039-5.
63. Götze, J.; Kempe, U. Physical Principles of Cathodoluminescence (CL) and its Applications in Geosciences. In *Cathodoluminescence and Its Application in the Planetary Sciences*; Gucsik, A., Ed.; Springer: Berlin/Heidelberg, Germany, 2009; pp. 1–22, doi:10.1007/978-3-540-87529-1_1.
64. Burnham, A.; Bulanova, G.; Smith, C.; Whitehead, S.; Kohn, S.; Gobbo, L.; Walter, M. Diamonds from the Machado River alluvial deposit, Rondônia, Brazil, derived from both lithospheric and sublithospheric mantle. *Lithos* **2016**, *265*, 199–213.
65. Thomson, A.; Kohn, S.; Bulanova, G.; Smith, C.; Araujo, D.; Walter, M. Origin of sub-lithospheric diamonds from the Juina-5 kimberlite (Brazil): Constraints from carbon isotopes and inclusion compositions. *Contrib. Mineral. Petrol.* **2014**, *168*, 1081.
66. Araujo, D.; Gaspar, J.; Bulanova, G.; Smith, C.; Kohn, S.; Walter, M.; Hauri, E. Juina diamonds from kimberlites and alluvials: A comparison of morphology, spectral characteristics and carbon isotope composition. In *Proceedings of the 10th International Kimberlite Conference*; Springer India: New Delhi, India, 2013; Volume 2, pp. 255–269.

67. Howell, D.; Piazolo, S.; Dobson, D.P.; Wood, I.G.; Jones, A.P.; Walte, N.; Frost, D.J.; Fisher, D.; Griffin, W.L. Quantitative characterization of plastic deformation of single diamond crystals: A high pressure high temperature (HPHT) experimental deformation study combined with electron backscatter diffraction (EBSD). *Diam. Relat. Mat.* **2012**, *30*, 20–30, doi:10.1016/j.diamond.2012.09.003.
68. Evans, T.; Wild, R.K. Plastic deformation of diamond at temperatures below 1800 °C. *Philos. Mag.* **1966**, *13*, doi:10.1080/14786436608211997.